

Magnetic moiré surface states and flat chern band in topological insulators

Zhaochen Liu,¹ Huan Wang,¹ and Jing Wang^{1,2,3,*}

¹State Key Laboratory of Surface Physics and Department of Physics, Fudan University, Shanghai 200433, China

²Institute for Nanoelectronic Devices and Quantum Computing, Fudan University, Shanghai 200433, China

³Zhangjiang Fudan International Innovation Center, Fudan University, Shanghai 201210, China

(Dated: June 4, 2021)

We theoretically study the effect of magnetic moiré superlattice on the topological surface states by introducing a continuum model of Dirac electrons with a single Dirac cone moving in the time-reversal symmetry breaking periodic potential. The Zeeman-type moiré potentials generically gap out the moiré surface Dirac cones and give rise to isolated flat Chern minibands with Chern number ± 1 . This result provides a promising platform for realizing the time-reversal breaking correlated topological phases. In a C_6 periodic potential, when the scalar U_0 and Zeeman Δ_1 moiré potential strengths are equal to each other, we find that energetically the first three bands of Γ -valley moiré surface electrons are non-degenerate and realize i) an s -orbital model on a honeycomb lattice, ii) a degenerate p_x, p_y -orbitals model on a honeycomb lattice, and iii) a hybridized sd^2 -orbital model on a kagome lattice, where moiré surface Dirac cones in these bands emerge. When $U_0 \neq \Delta_1$, the difference between the two moiré potential serves as an effective spin-orbit coupling and opens a topological gap in the emergent moiré surface Dirac cones.

Introduction.—Recently, moiré superlattices in twisted two-dimensional (2D) materials provide a novel platform to study a variety of strong correlation effects in flat minibands. Two prime examples are twisted graphene and transition metal dichalcogenide (TMD) multilayers [1–5]. Motivated by the success of twisted van der Waals heterostructures, it is natural to study the effect of moiré superlattice of the Dirac cone on the surface of a 3D topological insulator (TI). Moiré superlattices in TI materials are ubiquitous, either in TI film grown on lattice mismatched substrate, or misalignment of topmost quintuple layer in bulk Bi_2Te_3 [6–13]. Previous studies have revealed the folded gapless Dirac cone within the bulk gap due to its topological nature from the time-reversal (TR) invariant moiré superlattice, where moiré surface states do not form isolated minibands [14–16]. Thus to introduce TR breaking is a natural step to obtain isolated and even topological moiré surface minibands. The incorporation of the magnetic proximity effect into topological surface states have significantly enriched the variety of quantum matter [17–19] exemplified in heterostructures with magnetic insulators [20–22] and intrinsic magnetic TI [23–29], in particular van der Waals MnBi_2Te_4 , which is compatible with the Bi_2Te_3 family materials [30]. Therefore it is straightforward to twist the van der Waals heterostructure of TI and magnetic insulator, while their effect on topological surface states have not been studied theoretically.

In this paper, we study the band structure of magnetic moiré surface states of TIs. Until now, all of the experimental moiré systems are TR invariant at the single particle level, thus the total Chern number is always equal to zero. Therefore, even with flat bands, it is quite difficult to achieve TR breaking interacting topological states such as the fractional Chern insulator in these systems. This motivates us to consider moiré superlattice of mag-

netic topological surface states. The topological nature of moiré surface Dirac cones is protected by TR symmetry, we find a Zeeman-type moiré potential generically opens the gap in the moiré surface Dirac cones and give rise to isolated flat Chern minibands with Chern number ± 1 . In a C_6 periodic potential, the Γ -valley moiré surface electrons simulate 2D honeycomb lattice physics, leading to emergent moiré surface Dirac cones.

Moiré Dirac electron.—We introduce and study a model of TI surface Dirac fermions in periodic scalar potential with TR breaking and analyze its normal band structure and topology in moiré Brillouin zone (MBZ). Now we start with the massless Dirac fermion with a single Dirac cone at Γ in 2D

$$\mathcal{H}_0(\mathbf{k}) = v_F (k_x \sigma_y - k_y \sigma_x), \quad (1)$$

where v_F is the Fermi velocity, $\boldsymbol{\sigma} = (\sigma_x, \sigma_y, \sigma_z)$ are Pauli matrices, $\mathbf{k} = (k_x, k_y)$ are the 2D momentum. A uniform exchange coupling between an out-of-plane magnetization and Dirac fermion opens a gap in the surface spectrum, and leads to the surface quantum Hall effect with a half-quantized Hall conductance. Now we put this Dirac fermion in a periodic TR breaking moiré potential $U(\mathbf{r})$ with a discrete translational symmetry, then to the lowest-order perturbation,

$$\mathcal{H} = \mathcal{H}_0(-i\partial_{\mathbf{r}}) + U(\mathbf{r}), \quad (2)$$

$$U(\mathbf{r}) = U_0(\mathbf{r})\sigma_0 + \Delta(\mathbf{r})\sigma_z, \quad (3)$$

where $U(\mathbf{r}) = U(\mathbf{r} + \mathbf{L}_{1,2})$, and $\mathbf{L}_{1,2}$ are two primitive vectors of the moiré superlattice, σ_0 is the identity matrix. $U_0(\mathbf{r})$ is the scalar potential, and $\Delta(\mathbf{r})$ is the Zeeman-type potential from magnetic exchange interaction which contains both the moiré and uniform parts. This model can apply to bulk TI crystal with twisted surface states in the interface between a TI and a ferromagnetic insulator.

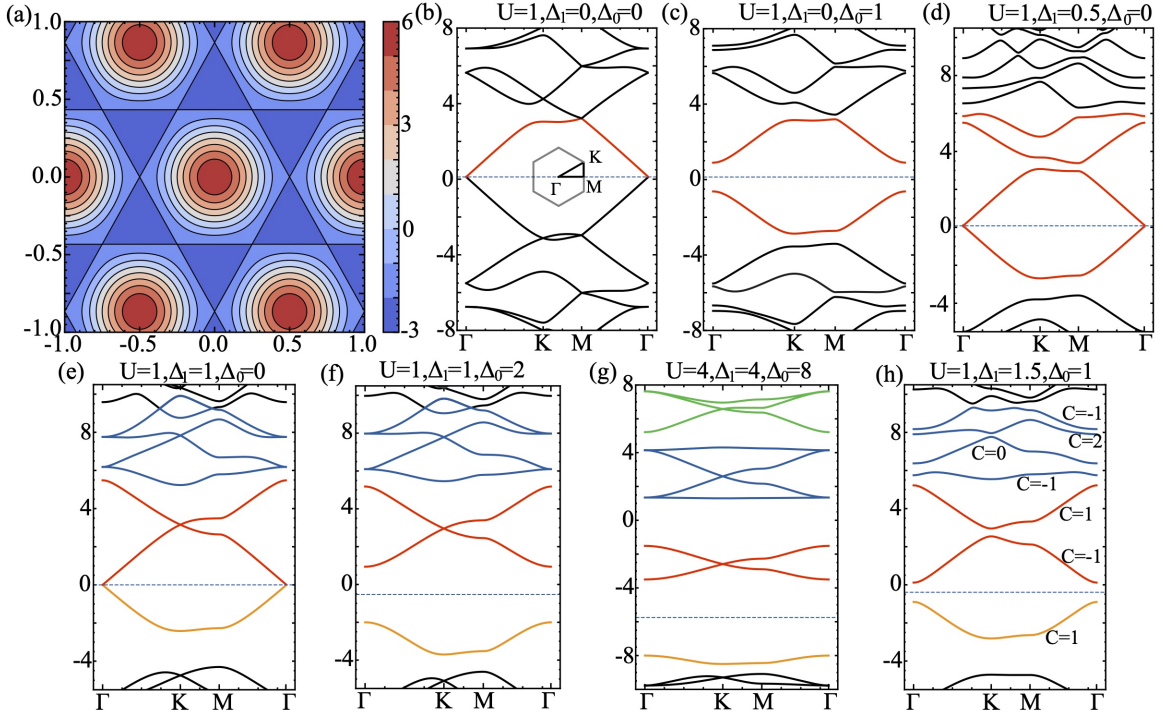


FIG. 1. (a) Schematic diagram of a C_6 moiré potential. (b) Energy spectrum at potential $(U_0, \Delta_1, \Delta_0) = (1, 0, 0)$. The corresponding MBZ is shown in the center. The entire spectrum remains gapless due to TR symmetry. The Dirac points are at Γ and M . The Zeeman moiré potential or uniform Zeeman term will generically gap out Dirac points as shown in (c,d) with $(U_0, \Delta_1, \Delta_0) = (1, 0, 1)$ and $(1, 0.5, 0)$, respectively. (e)-(g) When $U_0 = \Delta_1$, the first three conduction bands originate from s orbital, p_x, p_y orbitals at honeycomb lattice and sd^2 orbitals at kagome site. All these band structure has characteristic Dirac points at high symmetric points despite of finite Δ_0, Δ_1 . (h) $U_0 \neq \Delta_1$ effectively introduce spin-orbit coupling and introduces a topological gap, and each bands gain non-trivial Chern numbers. All parameters are in unit of v_F/L .

Although all of the physical effects discussed in this paper are generic for any magnetic moiré superlattice on topological surface states. To be concrete, we would like to start from a simple model describing the TIs of Bi_2Te_3 family [18], where threefold rotations with respect to the z -axis (C_{3z}) require that $U(\mathbf{r}) = U(C_{3z}\mathbf{r})$. We consider the periodic potential with a form

$$U(\mathbf{r}) = 2(U_0 + \Delta_1 \sigma_z) \sum_{j=1}^3 \cos(\mathbf{G}_j \cdot \mathbf{r}) + \Delta_0 \sigma_z, \quad (4)$$

where $\mathbf{G}_j = (4\pi/\sqrt{3}L)(-\sin(2\pi j/3), \cos(2\pi j/3))$ are three reciprocal vectors. $(U_0, \Delta_1, \Delta_0)$ are the moiré potential strength, which are scalar potential, Zeeman moiré potential, and uniform Zeeman term. There are two sets of energy scales v_F/L and $(U_0, \Delta_1, \Delta_0)$ in this system, and the low-energy physics is determined by the ratio between v_F/L and $(U_0, \Delta_1, \Delta_0)$. In particular, as we will see in the following, the interplay of moiré potential $(U_0, \Delta_1, \Delta_0)$ would give rise to different band topology.

Band structure.—The band structures are calculated by using the plane-wave expansion with a cutoff of 80 basis sets. First we estimate the energy scale in the system.

For a typical TI such as Bi_2Te_3 , the Dirac velocity is $v_F \approx 250 \text{ meV}\cdot\text{nm}$ [31, 32]. If we set the moiré lattice length as $L = 10 \text{ nm}$ with the twisted angle $\theta = a/L$, then the energy scale of $v_F/L = 25 \text{ meV}$. Thus, in the unit of v_F/L , we expect energy scale of the effective potential at moiré scale is at the order of tens of meV [33–36], namely Δ_0 is around $[0, 2]$, Δ_1 is $[0, 2]$, and U_0 from $[0, 2]$.

Fig. 1(a) is a schematic diagram of the C_6 moiré potential, and the minimum of potential constitutes a honeycomb lattice. We therefore expect the physics of the moiré band are generated by orbitals sitting on the honeycomb sites. In Fig. 1(b) with $(U_0, \Delta_1, \Delta_0) = (1, 0, 0)$, the moiré potential U_0 folds the surface Dirac bands, and due to TR symmetry, the moiré surface Dirac cones at Γ are preserved and satellite Dirac points are found at M points, which is consistent with previous study [15, 16]. Moreover, U_0 introduces the particle-hole asymmetry. Generically these minibands are non-degenerate, since they are from the spin-orbit coupled topological surface states. Now we study the effect of TR breaking potentials. By turning on a finite either Zeeman term Δ_0 or moiré potential Δ_1 , all the moiré Dirac cones are generically gapped as shown in Fig. 1(c) and Fig. 1(d), respectively.

In particular, when $U_0 = \Delta_1$, we find the re-emergence of the gapless moiré Dirac cones at K in conduction bands of different energies as shown in Fig. 1(e). As shown more clearer in Fig. 1(h), the first three conduction bands can be classified into three different groups. To reveal the nature of moiré band physics, we identify the symmetries and centers of the Wannier orbitals underlying the moiré bands by employ topological quantum chemistry [37]. We first compute the symmetry of the Bloch states and classifying them in terms of the irreducible representations of the little groups at the corresponding high symmetry points, and then compare the list of irreducible representations with the Elementary Band Representations (EBR) of the space group $P6mm$ listed on the Bilbao Crystallographic server [38–41]. The results are listed in Fig. 2. Consistent with the emergent honeycomb structure of the moiré potential, the first set of bands is formed by s orbital on the honeycomb lattice. These bands form a Dirac point at K and are topologically equivalent to the π bands of graphene except there is no spin degeneracy. The second set of bands, is formed

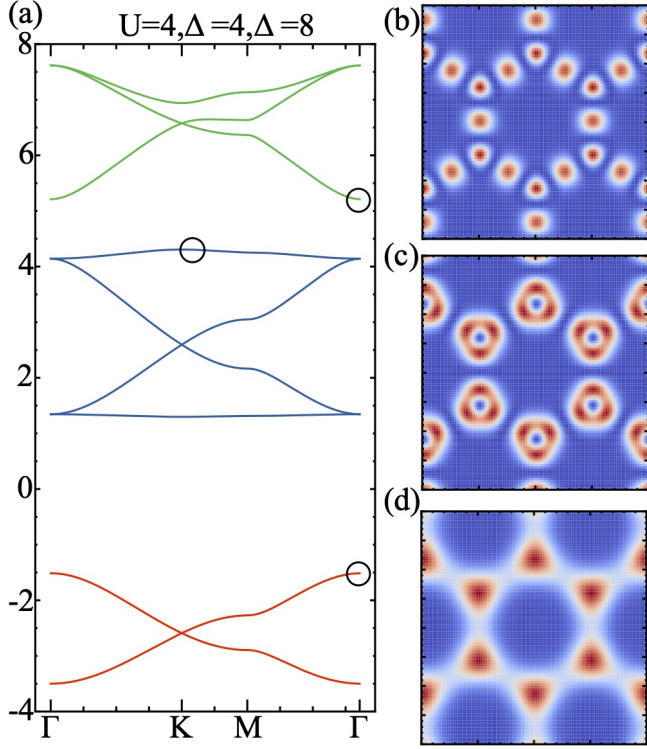


FIG. 2. (a) Energy spectrum with $(U_0, \Delta_1, \Delta_0) = (4, 4, 8)$. The three sets of bands originate from s Wannier orbitals on the honeycomb lattice, $p_x \pm ip_y$ Wannier orbitals on the honeycomb lattice, and hybridized sd^2 orbitals on the kagome lattice. (b)-(d) Wave function density distribution of three selected Bloch states encircled in (a), which clearly show the different orbital characters. Here we only present spin up part for the moiré potential only acts on spin up when $U = \Delta_1$.

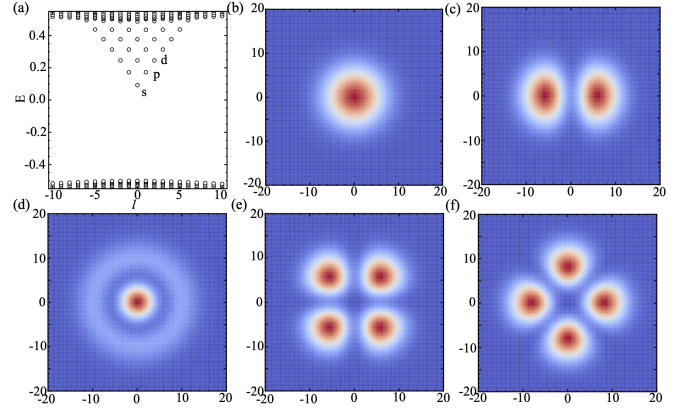


FIG. 3. (a) The bound states spectrum of Dirac fermion in the moiré potential valley. (b)-(f) The wave function density distributions of the bound states in energetic order show the s , p_x , d^2 , d_{xy} , $d_{x^2-y^2}$ orbitals characteristics. $(p_x \pm ip_y)$, $(d_{xy} \pm id_{x^2-y^2})$ are degenerate.

by $p_x \pm ip_y$ orbitals on an honeycomb [42, 43] that form a pair of almost dispersionless bands and also have a Dirac node at K . The third set of bands is formed by three bands which has one flat band and Dirac point at K . The symmetry analysis reveals that they are generated by orbitals centered on a kagome lattice, namely on the 3c Wyckoff positions lie at the mid bonds between two honeycomb sites. Such orbitals comes from hybridization of two different orbitals at honeycomb sites, which effectively transforms the hexagonal symmetry of the moiré lattice into the physics of the kagome lattice, namely the sd^2 graphene [44]. It is worth mentioning that similar results found in Γ -valley TMD moiré bands [36]. However, we point out there is an essential *difference* is that here the moiré bands are non-degenerate, and the Dirac points are emergent even in the presence of TR breaking at $U_0 = \Delta_1$ and are protected by C_{3v} . As we see in the following, when Δ_1 deviates from U_0 , the deviation effectively act as the spin-orbit coupling and opens a topological gap at Dirac points. While in Γ -valley TMD moiré bands, the Zeeman potential will not lead to gap opening but just split the spin up and down bands in energy. It is noted that for an opposite Zeeman potential, all similar physics will occur on highest in energy moiré valence bands when $U_0 = -\Delta_1$.

To illustrate how these orbitals emerges in the above moiré bands when $U_0 = \Delta_1$, we analyze the spectrum of Dirac fermion in a rotational invariant potential, namely $\mathcal{H}_0(-i\partial_{\mathbf{r}}) + \Delta_0\sigma_z + \Delta_1V(\mathbf{r})(\sigma_0 + \sigma_z)$. Thus the moiré potential only acts on spin up. We approximate the moiré potential near its minimum as a harmonic trap, $V(\mathbf{r}) \propto (\mathbf{r}/L)^2$ with a cutoff length of $R_0 \approx 0.2L$. Fig. 3(a) shows the energy spectrum from the numerical calculation performed on a disc geometry with radius $R = 4R_0$. There are bound states in the gap which are

classified into s , p , and d orbitals in energetic order, where their wave function density distributions for corresponding bound states are clearly demonstrated in Fig. 2(b)-(f). Thus the tight-binding model from hopping of the bound states at the honeycomb lattice naturally give rise to the above moiré bands.

Then we study the physics away from $U_0 = \Delta_1$. A typical spectrum is shown in Fig. 1(h) where the emergent Dirac points (as in Fig. 1(e-g)) are gapped, and one gets isolated flat bands. Such a gap opening must be topological as we can expect from EBR. We further calculate Chern number of the minibands which is well defined here, for the moiré potential regularizes the Dirac fermion into MBZ. As expected, these bands feature nontrivial Chern numbers. Furthermore, the $p_x \pm ip_y$ and $d_{xy} \pm id_{x^2-y^2}$ bound states are no longer degenerate when $U_0 \neq \Delta_1$. Therefore, the magnetic moiré potential $\delta = U_0 - \Delta_1$ (deviated from $U_0 = \Delta_1$) is an effective spin-orbit coupling and act as a topological mass term in the emergent Dirac bands [43], and the sign of Chern numbers is determined by the sign of δ . The bandwidth of the flat Chern band from p_x, p_y orbitals is about $\mathcal{W} \approx 0.2v_F/L$. Interestingly, the first pair of conduction bands essentially realize the Haldane mode on the honeycomb lattice [45], where the bandwidth is on the order of $\mathcal{W} \approx v_F/L$ and tuned by moiré lattice constant.

Now we understand the physics in magnetic moiré surface spectrum and band topology. We further calculate the Chern number phase diagram of the first conduction and valence bands as shown in Fig. 4. The phase boundary is obtained by finding the gap closing points. With

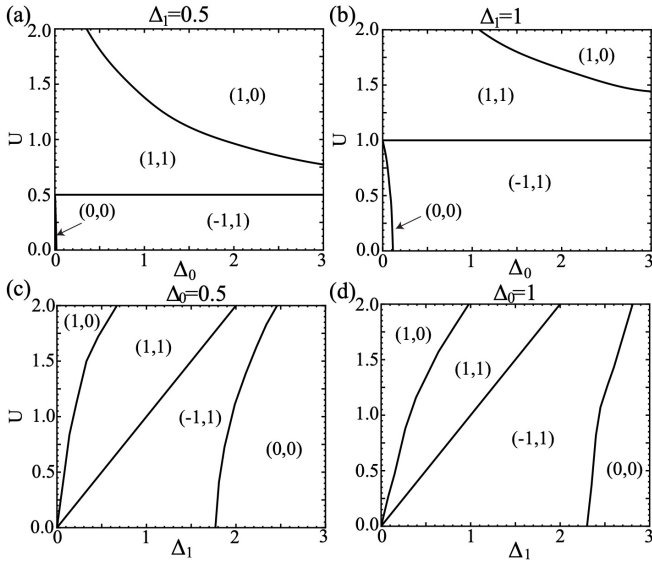


FIG. 4. Chern number phase diagram of the first conduction and valence bands (C_c, C_v) as function of (U, Δ_0) with $\Delta_1 = 0.5$ in (a) and $\Delta_1 = 1$ in (b). (c,d) (C_c, C_v) as function of (U, Δ_1) for $\Delta_0 = 0.5$ and $\Delta_0 = 1$, respectively.

a fixed Δ_0 , $(C_c, C_v) = (1, 0)$ when Δ_1 is small. The valence band will acquire a finite Chern number $C_v = 1$ from remote bands by increasing Δ_1 . When Δ_1 further increases, the conduction band will exchange Chern number with higher bands at K on $U = \Delta_1$ line and get $C_c = -1$. With further increasing Δ_1 , the conduction and valence bands become topological trivial by exchange Chern number with each other at Γ . As shown in Fig. 4(a,b) with a fixed Δ_1 , when Δ_0 is relatively small, the valence and conduction bands are always trivial when $U_0 < \Delta_1$. Similarly, as Δ_0 increases, the conduction and valence bands exchange Chern number with each other at Γ and becomes $(C_c, C_v) = (-1, 1)$. Now by crossing the $U_0 = \Delta_1$ line, the conduction band has $C_c = 1$ which exchanges Chern number at K with higher band. More results on the evolution of phase diagram are illustrated in Supplementary Materials [46].

Discussion.— The bandwidth of the flat Chern bands of moiré surface states is tuned by the twisting angle and is significantly smaller than the Coulomb repulsion energy, which make it an ideal platform for realizing interacting topological states [47–53]. For an estimation, taking the dielectric constant of TI surface states $\epsilon_r \approx 5$, one obtains a Coulomb interaction energy $\mathcal{U} = e^2/\epsilon_r L \approx 30$ meV. Thus $\mathcal{U}/\mathcal{W} \gtrsim 1$ for filling in the first sets of conduction/valence bands, while $\mathcal{U}/\mathcal{W} \gtrsim 6$ for filling in the second sets of conduction band. Furthermore, even with either Chern number 0 or ± 1 , the nondegenerate flat band allows a single Fermi surface with large density of states when partially filled, leading to a chance of realizing an intrinsic TR breaking superconductivity.

The band topology of lowest in energy magnetic moiré conduction bands is essentially rooted in the C_6 periodic potential for a simple realization of honeycomb lattice, which is the case for Bi_2Te_3 . In a D_4 periodic potential, one could also get flat Chern band but these interesting emergent Dirac cone from orbital-active models in biparticle lattice will not occur. Here we emphasize the results are different from previous study on twisted magnetic TI bilayer, there strong hybridization between top and bottom gapped surface states occurs [54].

Next we briefly discuss the superconducting proximity effect. Without the moiré potentials, the proximitized surface state is always a topological superconductor when $\Delta_0 < \Delta_s$ if $\mu = 0$ or $\mu > \Delta_0$, with Δ_s is the s -wave pairing amplitude. We find by adiabatically turning on the moiré potential, the band structure changes but without gap closing. Namely, the system is always in the topological superconducting state with above condition [46]. Therefore, Majorana zero mode in the vortex core and chiral Majorana edge modes are expected [55, 56].

Finally, we discuss the feasibility to realize our model of magnetic Dirac fermion in periodic potential. Mechanically robust single septuple layer of MnBi_2Te_4 has been obtained experimentally [57], making it possible to implement twisted superlattice on Bi_2Te_3 surfaces. The wave

function density of Dirac surface state resides in both MnBi_2Te_4 layer and topmost layer of Bi_2Te_3 [58], therefore both Δ_0 and Δ_1 are present. With the exchange coupling at the order of hundreds of meV, we expect the magnetic potential at moiré scale is at the order of tens of meV, namely $(U_0, \Delta_1, \Delta_0)$ is at the same order.

Summary.—We find the magnetic potentials generically gap out the moiré surface Dirac cones and lead to isolated flat Chern minibands with Chern number ± 1 , thus the fractional filling in it makes the strongly correlated topological states possible. The moiré surface electrons in a C_6 periodic potential simulate the physics of orbital-active honeycomb lattice, and the magnetic moiré potential acts as an effective spin-orbit coupling. Our model provides a convenient condensed matter platform to engineer the Haldane model with narrow bandwidth and strong interaction.

We acknowledge Y. Zhang for stimulating discussions. This work is supported by the National Key Research Program of China under Grant Nos. 2019YFA0308404 and 2016YFA0300703, the Natural Science Foundation of China through Grant No. 11774065, Shanghai Municipal Science and Technology Major Project under Grant No. 2019SHZDZX01, Science and Technology Commission of Shanghai Municipality under Grant No. 20JC1415900, and the Natural Science Foundation of Shanghai under Grant No. 19ZR1471400.

* wjingphys@fudan.edu.cn

- [1] Eva Y. Andrei and Allan H. MacDonald, “Graphene bilayers with a twist,” *Nature Mat.* **19**, 1265 (2020).
- [2] Leon Balents, Cory R. Dean, Dmitri K. Efetov, and Andrea F. Young, “Superconductivity and strong correlations in moiré flat bands,” *Nature Phys.* **16**, 725 (2020).
- [3] Stephen Carr, Shiang Fang, and Efthimios Kaxiras, “Electronic-structure methods for twisted moiré layers,” *Nature Rev. Mater.* **5**, 748 (2020).
- [4] R. Bistritzer and A. H. MacDonald, “Moiré bands in twisted double-layer graphene,” *Proc. Natl. Acad. Sci. U.S.A.* **108**, 12233–12237 (2011).
- [5] Y. Cao, V. Fatemi, S. Fang, K. Watanabe, T. Taniguchi, E. Kaxiras, and P. Jarillo-Herrero, “Unconventional superconductivity in magic-angle graphene superlattices,” *Nature* **556**, 43 (2018).
- [6] Can-Li Song, Yi-Lin Wang, Ye-Ping Jiang, Yi Zhang, Cui-Zu Chang, Lili Wang, Ke He, Xi Chen, Jin-Feng Jia, Yayu Wang, Zhong Fang, Xi Dai, Xin-Cheng Xie, Xiao-Liang Qi, Shou-Cheng Zhang, Qi-Kun Xue, and Xucun Ma, “Topological insulator bi_2se_3 thin films grown on double-layer graphene by molecular beam epitaxy,” *Appl. Phys. Lett.* **97**, 143118 (2010).
- [7] Yilin Wang, Yeping Jiang, Mu Chen, Zhi Li, Canli Song, Lili Wang, Ke He, Xi Chen, Xucun Ma, and Qi-Kun Xue, “Scanning tunneling microscopy of interface properties of bi_2se_3 on FeSe,” *J. Phys. Condens. Matter* **24**, 475604 (2012).
- [8] Jeong Heum Jeon, Won Jun Jang, Jong Keon Yoon, and Se-Jong Kahng, “Metal-supported high crystalline bi_2se_3 quintuple layers,” *Nanotechnology* **22**, 465602 (2011).
- [9] Y. Liu, Y. Y. Li, S. Rajput, D. Gilks, L. Lari, P. L. Galindo, M. Weinert, V. K. Lazarov, and L. Li, “Tuning dirac states by strain in the topological insulator bi_2se_3 ,” *Nature Phys.* **10**, 294 (2014).
- [10] Shuigang Xu, Yu Han, Xiaolong Chen, Zefei Wu, Lin Wang, Tianyi Han, Weiguang Ye, Huanhuan Lu, Gen Long, Yingying Wu, Jiangxiazhi Lin, Yuan Cai, K. M. Ho, Yuheng He, and Ning Wang, “van der waals epitaxial growth of atomically thin bi_2se_3 and thickness-dependent topological phase transition,” *Nano Lett.* **15**, 2645 (2015).
- [11] Jin-Peng Xu, Mei-Xiao Wang, Zhi Long Liu, Jian-Feng Ge, Xiaojun Yang, Canhua Liu, Zhu An Xu, Dandan Guan, Chun Lei Gao, Dong Qian, Ying Liu, Qiang-Hua Wang, Fu-Chun Zhang, Qi-Kun Xue, and Jin-Feng Jia, “Experimental detection of a majorana mode in the core of a magnetic vortex inside a topological insulator-superconductor $\text{bi}_2\text{te}_3/\text{nbse}_2$ heterostructure,” *Phys. Rev. Lett.* **114**, 017001 (2015).
- [12] Koen Schouteden, Zhe Li, Taishi Chen, Fengqi Song, Bart Partoens, Chris Van Haesendonck, and Kyungwha Park, “Moiré superlattices at the topological insulator bi_2te_3 ,” *Sci. Rep.* **6**, 20278 (2016).
- [13] Zachariah Hennighausen, Christopher Lane, Ioana Gianina Buda, Vineet K. Mathur, Arun Bansil, and Swastik Kar, “Evidence of a purely electronic two-dimensional lattice at the interface of $\text{tmd}/\text{bi}_2\text{se}_3$ heterostructures,” *Nanoscale* **11**, 15929 (2019).
- [14] Anthony Vargas, Fangze Liu, Christopher Lane, Daniel Rubin, Ismail Bilgin, Zachariah Hennighausen, Matthew DeCapua, Arun Bansil, and Swastik Kar, “Tunable and laser-reconfigurable 2d heterocrystals obtained by epitaxial stacking of crystallographically incommensurate bi_2se_3 and mos_2 atomic layers,” *Sci. Adv.* **3** (2017), 10.1126/sciadv.1601741.
- [15] Taige Wang, Noah F. Q. Yuan, and Liang Fu, “Moiré surface states and enhanced superconductivity in topological insulators,” *Phys. Rev. X* **11**, 021024 (2021).
- [16] Jennifer Cano, Shiang Fang, J. H. Pixley, and Justin H. Wilson, “Moiré superlattice on the surface of a topological insulator,” *Phys. Rev. B* **103**, 155157 (2021).
- [17] M. Z. Hasan and C. L. Kane, “Colloquium: Topological insulators,” *Rev. Mod. Phys.* **82**, 3045–3067 (2010).
- [18] Xiao-Liang Qi and Shou-Cheng Zhang, “Topological insulators and superconductors,” *Rev. Mod. Phys.* **83**, 1057–1110 (2011).
- [19] Yoshinori Tokura, Kenji Yasuda, and Atsushi Tsukazaki, “Magnetic topological insulators,” *Nat. Rev. Phys.* **1**, 126–143 (2019).
- [20] Peng Wei, Ferhat Katmis, Badih A. Assaf, Hadar Steinberg, Pablo Jarillo-Herrero, Donald Heiman, and Jagadeesh S. Moodera, “Exchange-coupling-induced symmetry breaking in topological insulators,” *Phys. Rev. Lett.* **110**, 186807 (2013).
- [21] Ferhat Katmis, Valeria Lauter, Flavio S. Nogueira, Badih A. Assaf, Michelle E. Jamer, Peng Wei, Biswarup Satpati, John W. Freeland, Ilya Eremin, Don Heiman, Pablo Jarillo-Herrero, and Jagadeesh S. Moodera, “A high-temperature ferromagnetic topological insulating phase by proximity coupling,” *Nature* **533**, 513–516 (2016).
- [22] Chi Tang, Cui-Zu Chang, Gejian Zhao, Yawen Liu,

- Zilong Jiang, Chao-Xing Liu, Martha R. McCartney, David J. Smith, Tingyong Chen, Jagadeesh S. Moodera, and Jing Shi, “Above 400-k robust perpendicular ferromagnetic phase in a topological insulator,” *Sci. Adv.* **3** (2017), 10.1126/sciadv.1700307.
- [23] Dongqin Zhang, Minji Shi, Tongshuai Zhu, Dingyu Xing, Haijun Zhang, and Jing Wang, “Topological axion states in the magnetic insulator mnbi_2te_4 with the quantized magnetoelectric effect,” *Phys. Rev. Lett.* **122**, 206401 (2019).
- [24] Mikhail M. Otrokov, Ilya I. Klimovskikh, Hendrik Bentmann, Alexander Zeugner, Ziya S. Aliev, Sebastian Gass, Anja U. B. Wolter, Alexander V. Koroleva, Dmitry Estyunin, Alexander M. Shikin, Maria Blanco-Rey, Martin Hoffmann, Alexander Yu. Vyazovskaya, Sergey V. Ere-meev, Yury M. Koroteev, Imamaddin R. Amiraslanov, Mahammad B. Babanly, Nazim T. Mamedov, Nadir A. Abdullayev, Vladimir N. Zverev, Bernd Büchner, Eike F. Schwier, Shiv Kumar, Akio Kimura, Luca Petaccia, Giovanni Di Santo, Raphael C. Vidal, Sonja Schatz, Katharina Kißner, Chul-Hee Min, Simon K. Moser, Thiago R. F. Peixoto, Friedrich Reinert, Arthur Ernst, Pedro M. Echenique, Anna Isaeva, and Evgueni V. Chulkov, “Prediction and observation of an antiferromagnetic topological insulator,” *Nature* **576**, 416–422 (2019).
- [25] Jiaheng Li, Yang Li, Shiqiao Du, Zun Wang, Bing-Lin Gu, Shou-Cheng Zhang, Ke He, Wenhui Duan, and Yong Xu, “Intrinsic magnetic topological insulators in van der waals layered mnbi_2te_4 -family materials,” *Sci. Adv.* **5**, eaaw5685 (2019).
- [26] Yan Gong, Jingwen Guo, Jiaheng Li, Kejing Zhu, Menghan Liao, Xiaozhi Liu, Qinghua Zhang, Lin Gu, Lin Tang, Xiao Feng, Ding Zhang, Wei Li, Canli Song, Lili Wang, Pu Yu, Xi Chen, Yayu Wang, Hong Yao, Wenhui Duan, Yong Xu, Shou-Cheng Zhang, Xucun Ma, Qi-Kun Xue, and Ke He, “Experimental realization of an intrinsic magnetic topological insulator,” *Chin. Phys. Lett.* **36**, 076801 (2019).
- [27] Jiazhen Wu, Fucui Liu, Masato Sasase, Koichiro Ienaga, Yukiko Obata, Ryu Yukawa, Koji Horiba, Hiroshi Kumigashira, Satoshi Okuma, Takeshi Inoshita, and Hideo Hosono, “Natural van der waals heterostructural single crystals with both magnetic and topological properties,” *Sci. Adv.* **5** (2019), 10.1126/sciadv.aax9989.
- [28] J.-Q. Yan, Y. H. Liu, D. S. Parker, Y. Wu, A. A. Aczel, M. Matsuda, M. A. McGuire, and B. C. Sales, “A-type antiferromagnetic order in mnbi_4te_7 and $\text{mnbi}_6\text{te}_{10}$ single crystals,” *Phys. Rev. Materials* **4**, 054202 (2020).
- [29] Chaowei Hu, Lei Ding, Kyle N. Gordon, Barun Ghosh, Hung-Ju Tien, Haoxiang Li, A. Garrison Linn, Shang-Wei Lien, Cheng-Yi Huang, Scott Mackey, Jinyu Liu, P. V. Sreenivasa Reddy, Bahadur Singh, Amit Agarwal, Arun Bansil, Miao Song, Dongsheng Li, Su-Yang Xu, Hsin Lin, Huibo Cao, Tay-Rong Chang, Dan Dessau, and Ni Ni, “Realization of an intrinsic ferromagnetic topological state in $\text{mnbi}_8\text{te}_{13}$,” *Sci. Adv.* **6** (2020), 10.1126/sciadv.aba4275.
- [30] E. D. L. Rienks, S. Wimmer, J. Sánchez-Barriga, O. Caha, P. S. Mandal, J. Ruzicka, H. Steiner A. Ney, V. V. Volobuev, H. Groiss, M. Albu, G. Kothleitner, J. Michalicka, S. A. Khan, J. Minár, H. Ebert, G. Bauer, F. Freyse, A. Varykhalov, O. Rader, and G. Springholz, “Large magnetic gap at the dirac point in $\text{bi}_2\text{te}_3/\text{mnbi}_2\text{te}_4$ heterostructures,” *Nature* **576**, 423 (2019).
- [31] Y. L. Chen, J. G. Analytis, J.-H. Chu, Z. K. Liu, S.-K. Mo, X. L. Qi, H. J. Zhang, D. H. Lu, X. Dai, Z. Fang, S. C. Zhang, I. R. Fisher, Z. Hussain, and Z.-X. Shen, “Experimental realization of a three-dimensional topological insulator, bi_2te_3 ,” *Science* **325**, 178–181 (2009).
- [32] Y. Xia, D. Qian, D. Hsieh, L. Wray, A. Pal, H. Lin, A. Bansil, D. Grauer, Y. S. Hor, R. J. Cava, and M. Z. Hasan, “Observation of a large-gap topological-insulator class with a single Dirac cone on the surface,” *Nature Phys.* **5**, 398–402 (2009).
- [33] A. Kerelsky, L. J. McGilly, D. M. Kennes, L. Xian, M. Yankowitz, S. Chen, K. Watanabe, T. Taniguchi, J. Hone, C. Dean, A. Rubio, and A. N. Pasupathy, “Maximized electron interactions at the magic angle in twisted bilayer graphene,” *Nature* **572**, 95 (2019).
- [34] F. Wu, T. Lovorn, E. Tutuc, I. Martin, and A. H. MacDonald, “Topological insulators in twisted transition metal dichalcogenide homobilayers,” *Phys. Rev. Lett.* **122**, 086402 (2019).
- [35] Yang Zhang, Noah F. Q. Yuan, and Liang Fu, “Moiré quantum chemistry: Charge transfer in transition metal dichalcogenide superlattices,” *Phys. Rev. B* **102**, 201115 (2020).
- [36] Mattia Angeli and Allan H MacDonald, “ γ valley transition metal dichalcogenide moiré bands,” *Proc. Natl. Acad. Sci. U.S.A.* **118**, e2021826118 (2021).
- [37] Barry Bradlyn, L Elcoro, Jennifer Cano, MG Vergniory, Zhijun Wang, C Felser, MI Aroyo, and B Andrei Bernevig, “Topological quantum chemistry,” *Nature* **547**, 298 (2017).
- [38] J. Perez-Mato, D Orobengoa, Emre Tasci, Gemma De la Flor Martin, and A Kirov, “Crystallography online: Bilbao crystallographic server,” *Bulg. Chem. Commun.* **43**, 183–197 (2011).
- [39] MI Aroyo, JM Perezmato, C Capillas, E Kroumova, Svetoslav Ivantchev, G Madariaga, A Kirov, and Hans Wondratschek, “Bilbao crystallographic server: I. databases and crystallographic computing programs,” *Z. Krist.* **221**, 15–27 (2006).
- [40] Asen Kirov, Cesar Capillas, J Perez-Mato, and Hans Wondratschek, “Bilbao crystallographic server. ii. representations of crystallographic point groups and space groups,” *Acta Cryst.* **62**, 115–28 (2006).
- [41] L. Elcoro, Barry Bradlyn, Z. Wang, M. G. Vergniory, Jennifer Cano, C. Felser, B. Bernevig, D. Orobengoa, G. D. L. Flor, and M. Aroyo, “Double crystallographic groups and their representations on the bilbao crystallographic server,” *J. Appl. Crystallogr* **50**, 1457 (2017).
- [42] Congjun Wu, Doron Bergman, Leon Balents, and S. Das Sarma, “Flat bands and wigner crystallization in the honeycomb optical lattice,” *Phys. Rev. Lett.* **99**, 070401 (2007).
- [43] Huan Wang and Jing Wang, “Topological bands in two-dimensional orbital-active bipartite lattices,” *Phys. Rev. B* **103**, L081109 (2021).
- [44] Miao Zhou, Zheng Liu, Wenmei Ming, Zhengfei Wang, and Feng Liu, “ sd^2 graphene: Kagome band in a hexagonal lattice,” *Phys. Rev. Lett.* **113**, 236802 (2014).
- [45] F. D. M. Haldane, “Model for a quantum hall effect without landau levels: Condensed-matter realization of the “parity anomaly,”” *Phys. Rev. Lett.* **61**, 2015–2018 (1988).
- [46] See Supplemental Material for more details.

- [47] M. Levin and A. Stern, “Fractional topological insulators,” *Phys. Rev. Lett.* **103**, 196803 (2009).
- [48] Joseph Maciejko, Xiao-Liang Qi, H. Dennis Drew, and Shou-Cheng Zhang, “Topological quantization in units of the fine structure constant,” *Phys. Rev. Lett.* **105**, 166803 (2010).
- [49] X.-L. Qi, “Generic wave-function description of fractional quantum anomalous hall states and fractional topological insulators,” *Phys. Rev. Lett.* **107**, 126803 (2011).
- [50] E. Tang, J.-W. Mei, and X.-G. Wen, “High-temperature fractional quantum hall states,” *Phys. Rev. Lett.* **106**, 236802 (2011).
- [51] K. Sun, Z. Gu, H. Katsura, and S. Das Sarma, “Nearly flatbands with nontrivial topology,” *Phys. Rev. Lett.* **106**, 236803 (2011).
- [52] T. Neupert, L. Santos, C. Chamon, and C. Mudry, “Fractional quantum hall states at zero magnetic field,” *Phys. Rev. Lett.* **106**, 236804 (2011).
- [53] E. M. Spanton, A. A. Zibrov, H. Zhou, T. Taniguchi, K. Watanabe, M. P. Zaletel, and A. F. Young, “Observation of fractional chern insulators in a van der waals heterostructure,” *Science* **360**, 62–66 (2018).
- [54] Biao Lian, Zhaochen Liu, Yuanbo Zhang, and Jing Wang, “Flat chern band from twisted bilayer mnbi_2te_4 ,” *Phys. Rev. Lett.* **124**, 126402 (2020).
- [55] Liang Fu and C. L. Kane, “Superconducting proximity effect and majorana fermions at the surface of a topological insulator,” *Phys. Rev. Lett.* **100**, 096407 (2008).
- [56] Jing Wang, Quan Zhou, Biao Lian, and Shou-Cheng Zhang, “Chiral topological superconductor and half-integer conductance plateau from quantum anomalous hall plateau transition,” *Phys. Rev. B* **92**, 064520 (2015).
- [57] Yujun Deng, Yijun Yu, Meng Zhu Shi, Zhongxun Guo, Zihan Xu, Jing Wang, Xian Hui Chen, and Yuanbo Zhang, “Quantum anomalous hall effect in intrinsic magnetic topological insulator mnbi_2te_4 ,” *Science* **367**, 895–900 (2020).
- [58] M. M. Otrokov, T. V. Menshchikova, M. G. Vergniory, I. P. Rusinov, A. Yu. Vyazovskaya, Yu. M. Koroteev, G. Bihlmayer, A. Ernst, P. M. Echenique, A. Arnau, and E. V. Chulkov, “Highly-ordered wide bandgap materials for quantized anomalous Hall and magnetoelectric effects,” *2D Mater.* **4**, 025082 (2017).